Surface Adatom Diffusion-Assisted Dislocation Nucleation in Metal Nanowires

Lijie He,[†] Guangming Cheng,[‡] Yong Zhu,[‡] and Harold S. Park[*,†]

†*Department of Mechanical Engineering, Boston University, Boston, MA 02215, USA*

‡*Department of Mechanical and Aerospace Engineering, North Carolina State University, Raleigh, NC 27695, USA.*

E-mail: parkhs@bu.edu

Abstract

We employ a hybrid diffusion/nucleation-based Kinetic Monte Carlo model to elucidate the significant impact of adatom diffusion on incipient surface dislocation nucleation in metal nanowires. We reveal a stress-regulated diffusion mechanism that promotes preferential accumulation of diffusing adatoms near nucleation sites, which explains the experimental observations of strong temperature but weak strain-rate dependence, as well as temperature-dependent scatter of the nucleation strength. Furthermore, the model demonstrates that decreasing adatom diffusion with increasing strain rate will lead to stress-controlled nucleation being the dominant nucleation mechanism at higher strain rates. Overall, our model offers new mechanistic insights as to how surface adatom diffusion directly impacts the incipient defect nucleation process, and resulting mechanical properties, of metal nanowires.

Keywords

Mechanical deformation, Plasticity, Surface Diffusion, Defects Nucleation, Nanostructures, Kinetic Monte Carlo

With the continuous development of experimental technologies such as in situ transmission electron microscopy (TEM)[1,2] in the past few decades, researchers have gained enormous knowledge on the relationship between defect nucleation and the subsequent plastic deformation of nanosized materials.[3–7] Due to their small dimensions, nano-sized crystalline structures are often synthesized to feature few to no pre-existing dislocations[8,9] rendering them dependent on the nucleation of fresh dislocations from their surfaces to relieve stress under plastic deformation. Molecular dynamics (MD) simulation studies have over the past two decades demonstrated that such surface nucleation events are only possible at ultra-high stresses approaching the theoretical strength.[10–13] Concurrently, in situ nanomechanical experiments have been conducted to observe and measure the nucleation events in defect-scarce nanomaterials.[8,14–24] The role of different types of point defects, e.g., vacancies[25] and hydrogen interstitials,[26] on the activation energy of surface dislocation nucleation have been investigated. Other studies have investigated and found evidence of the interplay between diffusive and displacive plasticity.[17–19] These studies have collectively shown a strong temperature-dependence and a weak strain-rate dependence of the dislocation nucleation strength at experimentally relevant strain rates ($10^{-5} \sim 10^{-1}/s$).

While these behaviors have been established, the atomistic origins of these effects remain unresolved. An intriguing idea that has been proposed[14] but not validated is that the strong temperature-dependence of the nucleation strength implies that pre-existing defects other than dislocations, such as surface self-diffusion of point defects, could serve as a precursor to the surface dislocation nucleation event itself.[14,17,18,25,26] Here, we have conducted kinetic Monte Carlo (KMC) studies to investigate the central hypothesis that diffusion of point defects plays a fundamental role in surface dislocation nucleation in pristine crystalline nanomaterials. In doing so, we elucidate specific mechanisms by which the diffusion

of a particular type of point defects, surface adatoms, directly impacts the incipient surface dislocation nucleation process.

We investigate Pd surface adatom diffusion-controlled incipient dislocation nucleation in truncated rhombic $\langle 1\bar{1}0 \rangle$ Pd nanowires, with diameters ranging from 4-20 nm, and lengths of 16.5 nm, with tensile loading along the $[1\bar{1}0]$ direction, as shown in Fig. 1 (a). The nanowires have (100) and (111) transverse surfaces, the intersections of which as shown in the red lines in Fig. 1 (a) represent preferential dislocation nucleation sites, or "nucleation edges", as previously shown in both MD simulations and experiments.[14,16] The overall KMC model comprises two separate, but coupled, KMC components. The first KMC component characterizes surface adatom diffusion, while the second KMC component characterizes surface dislocation nucleation. The two KMC components are coupled because the activation energy for surface dislocation nucleation depends on the relative position of the surface adatom to the nucleation edges, which is determined by the KMC model of surface adatom diffusion. *The KMC simulations do not account for structural relaxation after adatom diffusion, which could be accounted for by coupling MD and KMC.* Each simulation maintains a constant system temperature (T) and tensile loading strain rate ($\dot{\epsilon}$). We maintain a constant areal surface adatom density of $1.7 \times 10^{11}/cm^2$, ensuring the presence of at least one adatom in the smallest structures examined. For a 20 nm thick nanowire, this density corresponds to 5 adatoms per nanowire. The main text focuses on the results obtained from the 20 nm thick nanowire, while the supplemental information (SI) provides a brief discussion and results on nanowires with varying thicknesses.

In experiments, adatom deposition is governed by a balance between kinetic and thermodynamic control.[9] At equilibrium (thermodynamic dominant conditions), adatoms tend to remain away from edges due to their high energy state. Based on this observation, we assume that at the start of each KMC run at zero applied external stress, the adatom(s) are within 1 nm of the center of the (111) plane. We note that at experimentally relevant strain rates ($10^{-5} \sim 10^{-1}/s$), the structure size, initial adatom distribution, and adatom density

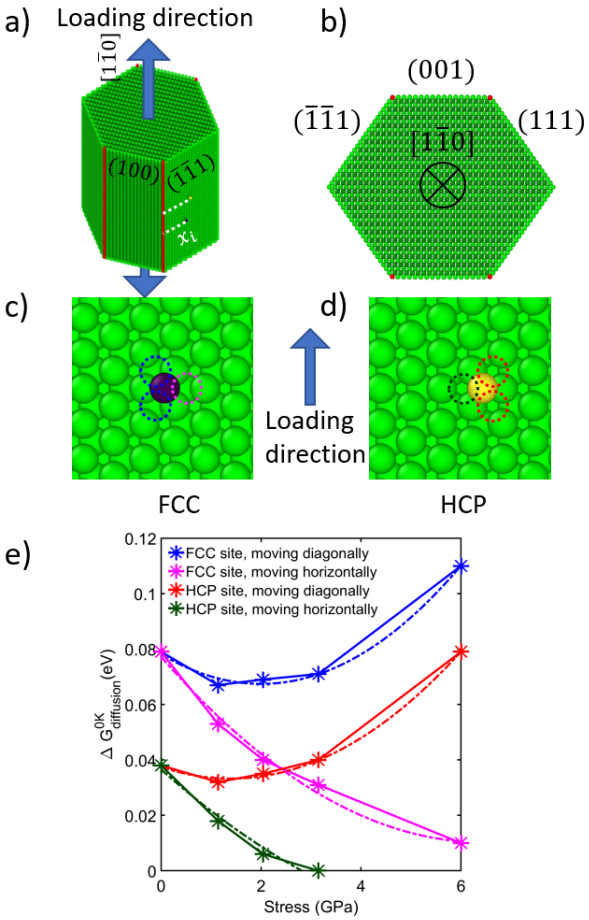

Figure 1: (a) Schematic representation of a $\langle 1\bar{1}0 \rangle$ oriented Pd nanowire used in the KMC simulation, featuring two adatoms situated near the center of the $(\bar{1}\bar{1}1)$ surface. The white dotted lines indicate the adatom locations x_i. The red lines on the front face and red dots on the back face denote potential dislocation nucleation sites under tensile stress when no adatoms are present. These sites are situated along intersecting edges between {100} and {111} surfaces. (b) Cross-sectional view of the Pd nanowire (adatoms not shown). (c) and (d) illustrate potential diffusion sites for adatoms when positioned on an FCC or HCP site. (e) Zero-temperature activation energy for diffusion, with the line color matching the site color in (c) and (d). Dotted curves represent fitted curves of the respective CINEB simulation results.

have minimal impact on the results, provided there is at least one adatom. However, for higher strain rates (i.e. $\dot{\epsilon} = 1/s$), these factors becomes increasingly important, particularly at lower temperatures. This will be discussed later in the context of strain rate sensitivity.

The diffusion and nucleation KMC components consist of multiple attempts. In the diffusion KMC, an attempt involves an adatom diffusing to an adjacent site, as shown in Figs. 1(c) and (d). If the attempt is successful, the new adatom position (x_i in Fig. 1 (a)) is updated. For the nucleation KMC, an attempt corresponds to forming a Shockley partial dislocation loop. If successful, the KMC simulation is terminated, and the current stress, σ, is deemed to be the nucleation strength.

Each adatom diffusion attempt or surface dislocation nucleation attempt uses its respective activation free energy to evaluate the probability (p) of an attempt's success:

$$p = min[1, e^{-\frac{1}{kT} \cdot \Delta G^{0K}_{attempt}(\sigma)(1-\frac{T}{T_m})}] \tag{1}$$

where k is the Boltzmann constant, T and σ represent the current simulation temperature and stress, respectively. The value p is then compared to a random number from a uniform distribution in the $(0, 1)$ interval. A successful attempt is when p is larger than the random number. T_m denotes the surface disordering temperature constant, where we use $T_m = 914$K for Pd.[14] The zero-temperature activation energy, $\Delta G^{0K}_{\text{attempt}}$, can be calculated using the Climbing Image Nudged Elastic Band (CINEB) method.[10,27] In this study, the Pd potential developed by Zhou et al.[28] has been utilized to perform the CINEB calculations. We direct readers to the SI for further details on the CINEB and KMC setup. As shown in Fig. 1 (e), $\Delta G^{0K}_{diffusion}(\sigma)$ is highly sensitive to the initial {111} site type (FCC site or HCP site) occupied by the adatom and the diffusion direction under applied tensile stress. In addition, $\Delta G^{0K}_{nucleation}(\sigma)$, illustrated in Fig. 2 (a), is influenced by the adatom's location, which is determined by the diffusion component of the KMC and then used as input for the nucleation KMC.

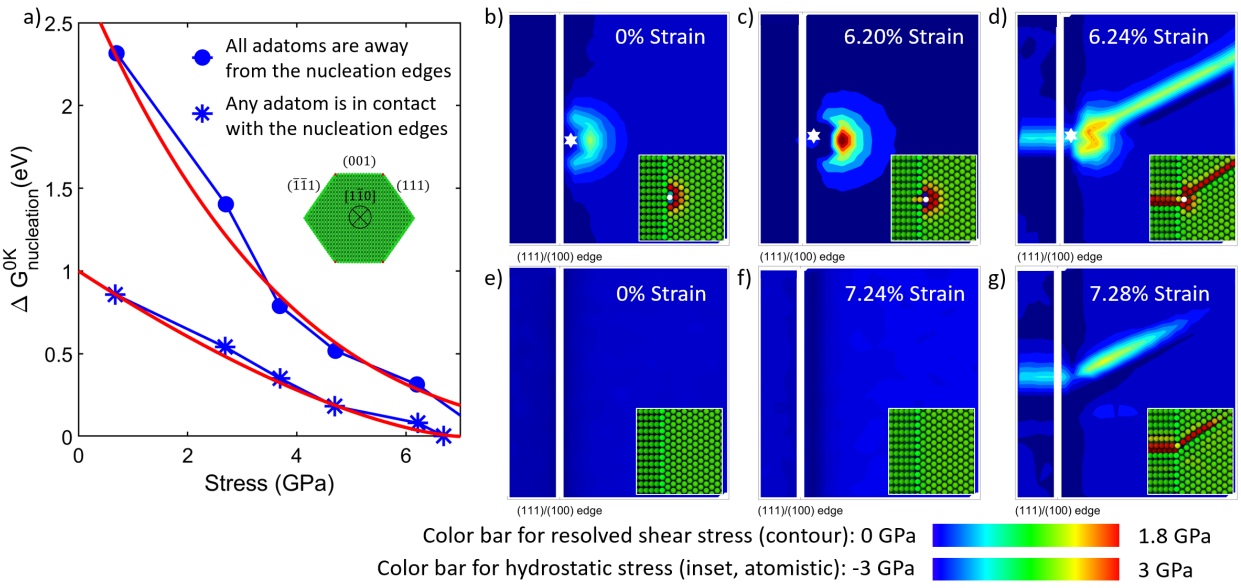

Figure 2: (a) Zero-temperature activation energy for surface dislocation nucleation based on adatom location. The inset shows the nanowire cross-section, with red dots indicating the (100)/(111) nucleation edges. The red curves are fitting curves based on CINEB simulation results. (b) - (d) Resolved shear stress contours near nucleation edges during MD tensile loading simulation with an adatom present (white hexagrams represent adatoms). (e) to (g) Resolved shear stress contours near nucleation edges during MD tensile loading simulation without an adatom. Insets in (b) to (g) display the corresponding atomic configurations color-coded by hydrostatic stress; the white atom in (b) to (d) marks the adatom location. White vertical lines in the figures highlight the (100)/(111) nucleation edges.

The edges between intersecting {001} and {111} surfaces, referred to as "nucleation edges", are potential dislocation nucleation sites even in the absence of adatoms.[14,16] When an adatom is within 0.5 nm, i.e. in contact with a nucleation edge (see Fig. 2 (b)-(d) for an example), the activation free energy for dislocation nucleation is significantly reduced as shown in Fig. 2(a). This reduction can be attributed to the adatom's presence, which causes a substantial increase in local resolved shear stress from 0.11 GPa (Fig. 2 (e)) to 0.77 GPa (Fig. 2(b)) even without external strain. *This considerable increase in shear stress can be attributed to surface stress changes induced by the adatom.* Consequently, the local stress increase facilitates incipient plastic deformation via Shockley partial nucleation near the adatom, as observed in Fig. 2 (d). In contrast, without adatoms, incipient Shockley partial nucleation can occur at any location along the nucleation edge. Overall, as shown in Fig. 2(a), the $\Delta G^{0K}_{nucleation}(\sigma)$ used to evaluate nucleation attempts depends on the adatom's proximity to the nucleation edge - if the adatom is in contact (i.e. within 0.5 nm) of the nucleation edge, the higher stress-dependent activation energy in Fig. 2(a) is used, while if not in contact, the lower activation energy is employed. *We note that in our KMC simulations, adatoms are assumed to diffuse independently of each other during the diffusion phase. Furthermore, defect nucleation during the nucleation stage is assumed to occur in the presence of a single adatom.*

We note that the activation energies for nucleation, both with and without adatoms, exhibit differences not only in magnitude but also in their stress dependencies, as illustrated in Fig. 2 (a). For a direct comparison of stress dependence, we introduce the common exponential-dependence as[10,14]

$$\Delta G^{0K}_{nucleation}(\sigma) = \Delta U_{act}(1 - \frac{\sigma}{\sigma_{athermal}})^{\alpha}, \tag{2}$$

where $\sigma_{athermal}$ represents the athermal strength limit. In our KMC model, we obtain the value of α directly from the fitting curves in Fig. 2(a). In the absence of adatoms, α has

a value of 3.92, consistent with CINEB calculations on edge dislocation nucleation in a ⟨110⟩ oriented Cu nanowire under tension[10] without adatoms. Including adatoms, however, reduces α to 1.56, signifying a decreased stress-dependence.

This reduction in α stems from adatoms assisting Shockley partial nucleation, creating locally concentrated stress fields less sensitive to applied stress. As depicted in Fig. 2 (b) and (c), the local resolved shear stress around the adatom only increases from 0.77 GPa to 1.74 GPa before yielding, while the applied tensile stress rises from 0 GPa to 4.56 GPa. In contrast, when adatoms are absent, the applied tensile stress acts as the sole driving force for dislocation nucleation, leading to a higher stress-dependence.

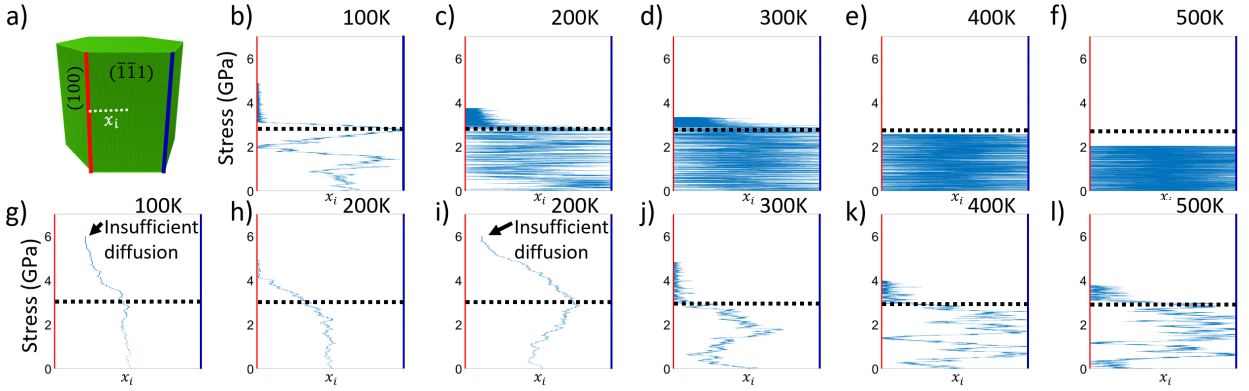

Figure 3: (a) Illustration of an adatom on a 20 nm diameter nanowire at the beginning of the KMC simulation. (b) - (f) Stress-dependent adatom diffusion trajectories leading to dislocation nucleation at various temperatures for strain rate $\dot{\epsilon} = 10^{-4}/s$. (g) - (l) Similar stress-dependent trajectories for strain rate $\dot{\epsilon} = 1/s$. *(h) shows the case where an adatom reaches the nucleation edge, facilitating nucleation, while (i) represents a scenario where the adatom does not reach the nucleation edge to facilitate nucleation, with both cases occurring under the same strain rate and temperature.* Although multiple adatoms diffuse on each nanowire due to the constant adatom density and larger nanowire diameter, only one trajectory is plotted for clarity. Black dashed lines denote the critical adatom trapping stress, from Fig. 1(e). Vertical red lines denote the (100)/(111) edges, and vertical blue lines denote the (111)/(111) edges.

Having established the KMC diffusion and nucleation models, we can now discuss the new mechanistic insights they offer into the role of surface diffusion on surface dislocation nucleation. Specifically, Fig. 1 (e) demonstrates that for tensile stresses exceeding about 3.1 GPa, $\Delta G^{0K}_{diffusion}(\sigma)$ for an HCP site adatom moving horizontally becomes zero and remains

so, indicating that adatoms will prefer to diffuse in a specific direction (e.g., to the left, following the site/direction schematic notations in Fig. 1 (c) and (d) as well as Fig. 3). This preferential movement ultimately leads to adatoms being "trapped" near nucleation edges when the applied stress exceeds the critical stress.

The critical stress for adatom trapping depends on nanowire size and temperature and is typically around 3 GPa for the considered nanowire diameters (5-20 nm). For the experimentally-relevant strain rates of $10^{-5} \sim 10^{-1}/s$, Fig. 3(b-f) illustrates how, for a given temperature, an individual adatom diffuses along the surface as a function of the applied tensile stress. Specifically, the adatoms tend to diffuse across the entire {111} surface numerous times before reaching the critical stress. However, when approaching or exceeding the critical stress, adatoms become trapped near nucleation edges due to the emergence of preferential diffusion directions. This trapping process significantly reduces the activation energy for surface dislocation nucleation, as shown in Fig. 2 (a). *Interestingly, we also found that the decrease in activation energy facilitated by surface adatoms is dependent on nanowire diameter and surface morphology, and further that this effect becomes smaller as the nanowire edges become more rounded. However, it is important to note that this effect does not entirely vanish, even in the extreme case of nanowires with round cross-sections.*

At strain rates of $10^{-5} \sim 10^{-1}/s$ in Figs. 3(b-f), the trapping mechanism exhibits temperature sensitivity, as the likelihood of thermally-induced events enabling adatoms to diffuse away from nucleation edges decreases at lower temperatures. As a result, Figs. 3(b-d) demonstrate a closer trapping of adatoms near nucleation edges at lower temperatures, which promotes yielding through adatom-facilitated nucleation events. Conversely, the trapping mechanism becomes less prominent at higher temperatures (400K and 500K in Figs. 3(d-e)) due to a combination of lower yielding stress and a higher probability of diffusive events in all directions.

While the trapping mechanism becomes less dominant at higher temperatures, the high diffusion attempt frequency (approximately 10^{12} attempts per second, calculation details

in the SI) and higher likelihood of diffusion events being accepted at higher temperatures enables adatoms to frequently reach the nucleation edges at higher temperatures. In conjunction with the high dislocation nucleation attempt frequency and the significant reduction in nucleation activation energy due to the presence of adatoms, this implies that adatom-facilitated nucleation events still dominate the yielding of nanowires at higher temperatures. In fact, all successful nucleation events at low strain rates ($10^{-5} \sim 10^{-1}/s$) in our KMC simulations involve adatoms in contact with the nucleation edges (i.e., adatom-facilitated nucleation events).

We now discuss the impact of strain rate on the stress-regulated diffusion mechanism, where Figs. 3 (g-l) illustrates the distinct behavior that occurs starting at a strain rate of about $1/s$. Higher-temperature results (300K, 400K and 500K) only show adatom-facilitated nucleation events resulting from occurrence of the adatom trapping mechanism, mirroring the low strain rate outcomes in Figs. 3 (b-f). However, at 200K, no-adatom-facilitated events begin to emerge, becoming equally as favorable as adatom-facilitated events. This is because with increasing strain rate, fewer diffusion attempts can occur before the applied stress reaches a level where the activation energy for nucleation without adatoms becomes sufficiently low, making it challenging for adatoms to reach the nucleation edge before stress-induced yielding occurs. *This transition arises as a consequence of the increasing strain rate, which reduces the time for diffusion before the applied stress attains a level at which the activation energy for nucleation without adatoms becomes sufficiently low. In other words, it becomes harder for adatoms to reach the nucleation edge prior to stress-induced yielding as the strain rate increases. This contrasts starkly with a strain rate of $10^{-4}/s$, where the nanowire takes 10,000 times longer to achieve the same strain as at a strain rate of $1/s$. This elongated period allows surface adatoms ample time to diffuse, enabling extended back-and-forth movement along the surface. Consequently, the wider diffusion range observed at a strain rate of $10^{-4}/s$, compared to $1/s$, is a direct result of this prolonged diffusion opportunity. We thus predict that an increase in strain rates above $1/s$ would further elevate*

the temperature threshold for the dominance of stress-induced nucleation events, as compared to adatom-facilitated nucleation events.

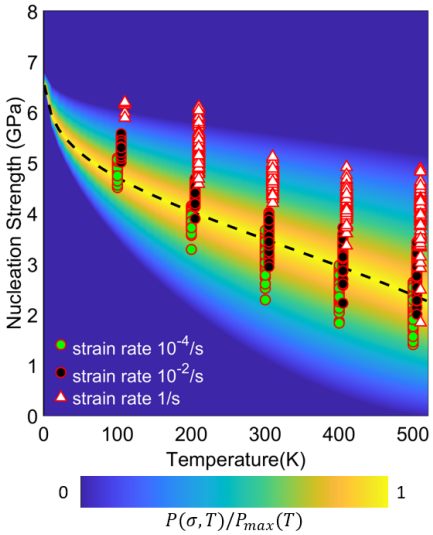

Figure 4: The predicted nucleation strength under varying temperature and strain rates from the KMC model. The background color map illustrates the temperature-dependent normalized probability distribution function, while the dashed black line indicates the most probable nucleation strength, both based on the analytical model proposed by Chen et al.[14] for a strain rate of $10^{-4}/s$ *and* $\alpha = 4$. Probability values $P(\sigma, T)$ are normalized in relation to the highest probability at each specific temperature ($P_{max}(T)$)

We note that the nucleation strength prediction of the KMC diffusion + nucleation model, as illustrated in Fig. 4, demonstrates reasonable agreement with both the experimental data and the analytical model from Chen et al.[14] for truncated-rhombic Pd nanowires at a similar strain rate ($\sim 10^{-4}/s$). Furthermore, the KMC model captures key features previously observed experimentally,[14] such as the high nucleation strength approaching the theoretical limit at low temperatures, the weak strain rate dependence from $10^{-4} \sim 10^{-3}/s$, and the significant scattering of nucleation strength due to the temperature-driven stochastic nature of the adatom-controlled surface dislocation nucleation process. As the strain rate increases to the transitional strain rate ($1/s$), a shift in nucleation strength occurs due to the relative lack of adatom diffusion discussed earlier. This effect is particularly evident at 200K, where both adatom-facilitated and no-adatom-facilitated nucleation events occur with similar ratios, resulting in further scattering in nucleation strength as seen in Fig. 4. *Furthermore,*

by taking the derivative of $\Delta G_{nucleation}$ with respect to stress σ, we are able to determine the changes in activation volumes[10,29] for the two distinct nucleation energy curves displayed in Fig. 2(a). We find that the activation volume for adatom-facilitated nucleation falls within the range of $1 - 10\ b^3$. Similarly, for nucleation that occurs without adatom facilitation, the activation volume ranges from $1 - 5\ b^3$. This indicates that in both cases, nucleation originates from a surface source as opposed to a bulk source such as the Frank-Read source, which typically involves activation volumes between $100 - 1000\ b^3$.

Finally, we note that our current study primarily examines truncated rhombic Pd nanowires. However, the generality of our findings for other FCC metals depends on the condition that the energy barrier for diffusion, as shown in Fig. 1(e), decreases to zero as the applied stress increases, thereby facilitating the adatom trapping mechanism discussed in this work. Preliminary results indicate that the energy barrier for diffusion decreasing to zero with increasing stress is found for a wide range of stacking fault energies. Thus, we anticipate that the exact nature of the initial nucleation event should not significantly affect the relevance of our conclusions for other FCC metals.

In summary, we have developed a kinetic Monte Carlo (KMC) model to investigate the previously proposed hypothesis of temperature or diffusion-assisted defect nucleation in truncated rhombic Pd nanowires. By capturing the fact that the diffusion of adatoms becomes directionally-biased at a critical applied stress level, we provide mechanistic understanding of experimental observations of high temperature-dependence and low strain-rate dependence at experimentally relevant strain rates ($10^{-5} \sim 10^{-1}/s$), as well as the temperature-dependent scatter in the surface dislocation nucleation strength. Furthermore, the model demonstrates that decreasing adatom diffusion with increasing strain rate will lead to stress-controlled nucleation being the dominant nucleation mechanism at higher strain rates. Overall, we demonstrate the significant influence that adatom diffusion can have on the incipient defect nucleation process in metal nanowires.

Acknowledgement

All authors acknowledge the support of the National Science Foundation, grant CMMI-1929651 *and CMMI-1929646*.

Supporting Information Available

Our supplementary information includes detailed descriptions of the CINEB and KMC setups used in our study, as well as a brief discussion of the size effect. This material is available free of charge via the Internet at `http://pubs.acs.org/`.

References

(1) Hirsch, P. B.; Horne, R. W.; Whelan, M. J. *Philosophical Magazine* **1956**, *1*.

(2) Minor, A. M.; Dehm, G. *MRS Bulletin* **2019**, *44*.

(3) Lu, Y.; Song, J.; Huang, J. Y.; Lou, J. *Nano Research* **2011**, *4*.

(4) Jennings, A. T.; Li, J.; Greer, J. R. *Acta Materialia* **2011**, *59*.

(5) Zheng, H.; Cao, A.; Weinberger, C. R.; Huang, J. Y.; Du, K.; Wang, J.; Ma, Y.; Xia, Y.; Mao, S. X. *Nature Communications* **2010**, *1*.

(6) Schuh, C. A.; Mason, J. K.; Lund, A. C. *Nature Materials* **2005**, *4*.

(7) Oh, S. H.; Legros, M.; Kiener, D.; Dehm, G. *Nature Materials* **2009**, *8*.

(8) Richter, G.; Hillerich, K.; Gianola, D. S.; MÃűnig, R.; Kraft, O.; Volkert, C. A. *Nano Letters* **2009**, *9*.

(9) Xia, Y.; Xia, X.; Peng, H. C. *Journal of the American Chemical Society* **2015**, *137*.

(10) Zhu, T.; Li, J.; Samanta, A.; Leach, A.; Gall, K. *Physical Review Letters* **2008**, *100*.

(11) Li, J.; Vliet, K. J. V.; Zhu, T.; Yip, S.; Suresh, S. *Nature* **2002**, *418*.

(12) Warner, D. H.; Curtin, W. A. *Acta Materialia* **2009**, *57*.

(13) Park, H. S.; Gall, K.; Zimmerman, J. A. *Journal of the Mechanics and Physics of Solids* **2006**, *54*.

(14) Chen, L. Y.; He, M. R.; Shin, J.; Richter, G.; Gianola, D. S. *Nature Materials* **2015**, *14*.

(15) Chang, T. H.; Cheng, G.; Li, C.; Zhu, Y. *Extreme Mechanics Letters* **2016**, *8*.

(16) Yin, S.; Cheng, G.; Richter, G.; Gao, H.; Zhu, Y. *ACS Nano* **2019**, *13*.

(17) Zhong, L.; Sansoz, F.; He, Y.; Wang, C.; Zhang, Z.; Mao, S. X. *Nature Materials* **2017**, *16*.

(18) Ramachandramoorthy, R.; Wang, Y.; Aghaei, A.; Richter, G.; Cai, W.; Espinosa, H. D. *ACS Nano* **2017**, *11*.

(19) Sun, S.; Kong, D.; Li, D.; Liao, X.; Liu, D.; Mao, S.; Zhang, Z.; Wang, L.; Han, X. *ACS Nano* **2019**, *13*.

(20) Seo, J. H.; Yoo, Y.; Park, N. Y.; Yoon, S. W.; Lee, H.; Han, S.; Lee, S. W.; Seong, T. Y.; Lee, S. C.; Lee, K. B.; Cha, P. R.; Park, H. S.; Kim, B.; Ahn, J. P. *Nano Letters* **2011**, *11*.

(21) Seo, J. H.; Park, H. S.; Yoo, Y.; Seong, T. Y.; Li, J.; Ahn, J. P.; Kim, B.; Choi, I. S. *Nano Letters* **2013**, *13*.

(22) Lee, S.; Im, J.; Yoo, Y.; Bitzek, E.; Kiener, D.; Richter, G.; Kim, B.; Oh, S. H. *Nature Communications* **2014**, *5*.

(23) Cheng, G.; Yin, S.; Li, C.; Chang, T. H.; Richter, G.; Gao, H.; Zhu, Y. *Acta Materialia* **2020**, *196*.

(24) Cheng, G.; Yin, S.; Chang, T. H.; Richter, G.; Gao, H.; Zhu, Y. *Physical Review Letters* **2017**, *119*.

(25) Qin, Q.; Yin, S.; Cheng, G.; Li, X.; Chang, T. H.; Richter, G.; Zhu, Y.; Gao, H. *Nature Communications* **2015**, *6*.

(26) Yin, S.; Cheng, G.; Chang, T. H.; Richter, G.; Zhu, Y.; Gao, H. *Nature Communications* **2019**, *10*.

(27) Henkelman, G.; Uberuaga, B. P.; JÃşnsson, H. *Journal of Chemical Physics* **2000**, *113*.

(28) Zhou, X. W.; Johnson, R. A.; Wadley, H. N. G. *Phys. Rev. B* **2004**, *69*, 144113.

(29) Zhang, X.; Li, X.; Gao, H. *Acta Mechanica Sinica* **2017**, *33*, 792–800.

Graphical TOC Entry